Proceedings of the ASME 2024 19th International Manufacturing Science and Engineering Conference
MSEC2024
June 17-21, 2024, Knoxville, Tennessee

MSEC2024-125193

A Preliminary Investigation of Input Shaping to Reduce the Residual Vibration of a Wafer-Handling Robot

Yung-Chun Lin
University of Michigan
Ann Arbor, MI

Chen Qian
University of Michigan
Ann Arbor, MI

Shorya Awtar
University of Michigan
Ann Arbor, MI

Chinedum E. Okwudire
University of Michigan
Ann Arbor, MI

ABSTRACT

Frog-leg robots are widely used for wafer-handling in semiconductor manufacturing. A typical frog-leg robot uses a magnetic coupler to achieve contactless transmission of motion between its driving motors, which operate at atmospheric pressure, and its end effector (blade) which operates within a vacuum chamber. However, the magnetic coupler is a low-stiffness transmission element that induces residual vibration during fast motions of the robot. Excessive residual vibration can cause collisions between the fragile wafer carried by the robot and cassette, hence damaging the wafer. While this problem could be solved by slowing down the robot, it comes at the cost of reduced productivity, which is undesirable. Therefore, this paper reports a preliminary investigation into input shaping (a popular vibration compensation technique) as a tool to reduce residual vibration of a frog-leg robot during high-speed motions. Two types of motions of the robot are considered: rotation and extension. A standard input shaper is shown to be very effective for mitigating residual vibration caused by rotational motion but is much less effective for extensional motion. The rationale is that the resonance frequencies of the robot are constant during rotation but they vary significantly during extension, hence reducing the effectiveness of standard input shaping. This necessitates the use of more advanced input shapers that can handle varying resonance frequencies to mitigate residual vibration during extensional motion in future work.

Keywords: Semiconductor manufacturing, silicon wafer-handling, frog-leg robot, residual vibration, input shaping

1. INTRODUCTION

The semiconductor industry is the backbone of modern electronics, producing microchips and integrated circuits that power our devices. These chips often start as wafers, thin, fragile, and highly valuable substrates. During the manufacturing process, these wafers must be handled with extreme care and precision. To optimize this manufacturing operation, a certain type of robot, distinctively termed the "frog-leg" wafer-handling robot for its unique, leg-like appendages, is often deployed [1,2]. Nevertheless, much like their traditional counterparts, these robots are prone to residual vibration, ultimately leading to product flaws and sizeable financial ramifications.

Wafer-handling robots face key challenges, including residual vibration, where the robot overshoots and oscillates in the desired path when transporting wafers. The phenomenon can stem from various sources, including mechanical vibration, sudden accelerations, and control system limitations. Vibration not only jeopardizes product quality but can also lead to costly equipment damage. Traditional methods to reduce vibration often involve slowing down the robot's movements, which can hamper production efficiency [3]. Therefore, finding a solution that reduces residual vibration while maintaining production speed is a crucial pursuit in the semiconductor industry.

The proposed solution in this manuscript centers around the concept of "input shaping." Input shaping (IS) is a control technique used to reduce the vibration of dynamic systems [4]. It involves carefully designing and applying input commands or control signals to the robot in such a way that the vibration is canceled out, resulting in smoother and more accurate movements. The primary objective of this research is to investigate the feasibility and effectiveness of input shaping techniques for vibration suppression in wafer-handling robots. The research aims to provide a comprehensive analysis of the application of input shaping, highlighting its benefits, limitations, and potential challenges in the context of semiconductor manufacturing.

To the authors' best knowledge, there is no research in the open literature addressing vibration suppression of frog-leg robots using input shaping. Liu *et al*. [5] and Aribowo *et al*. [6] demonstrated the capability of input shaping to suppress vibration in wafer-handling robots. However, the multi-link semiconductor wafer-handling robot was utilized instead of a frog-leg robot that adopts a parallel structure. Wang *et al*. [7,8] deployed a closed loop vibration rejection method using vibrotactile transducers on similar wafer-handling robot in this study. Yu *et al.* [1] injected torque offset to the input in addition to a PID controller for optimal control.

The main contribution of this research lies in demonstrating the effectiveness of input shaping on reducing residual vibration while increasing the operational speed of a frog-leg robot that adopts parallel structure.

2. OVERVIEW OF WAFER-HANDLING SYSTEM

The wafer-handling setup for this research consists of a frog-leg robot, laser sensor, accelerometer, motor driver, target controller, and a host PC. The layout is shown in Fig. 1 (not including the accelerometer and host PC).

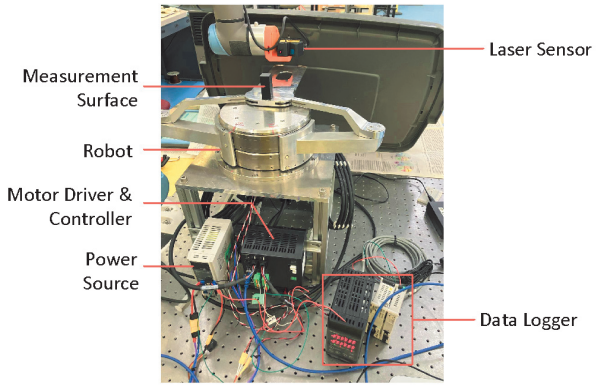

FIGURE 1: Setup to transport wafer using frog-leg robot

2.1 Frog-Leg Robot

The frog-leg robot is driven by two high precision stepper motors. The stepper motors are connected to a circular magnet retainer via a belt, which transmits the motion from the motor to the inner magnetic retainer. A schematic diagram illustrating this structure is shown in Fig. 2(a). Fig. 2(b) depicts how motion is transmitted from the inner magnet retainer to the outer retainer. The outer magnetic retainer is directly connected to the robot arm, which is equipped with a blade designed for carrying silicon wafers (see Figure 3).

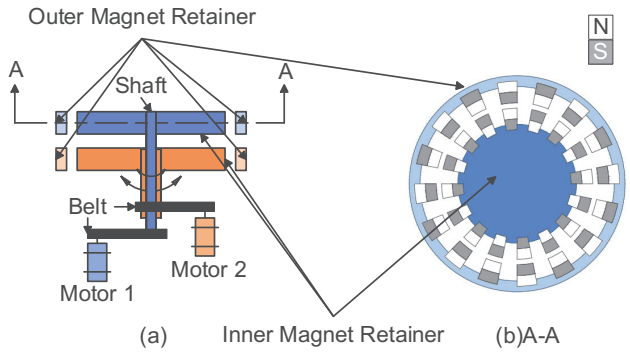

FIGURE 2: Schematic diagram of (a) side view of the interior of the robot; (b) top view of the inner and outer magnet retainer

The wafer-handling robot incorporates magnetic retainers with multiple pole pairs, allowing the inner magnetic retainers and the motors to operate within an atmospheric environment, while the wafers and outer magnetic retainers operate in vacuum. The magnetic retainers move in tandem with their respective motors, transmitting motion from the motors to the end effector. Due to the inherent lower stiffness of the magnetic pole pairs compared to the other pivot joints connecting the blade to the outer magnetic retainers, the robot oscillates around the center of the retainers after each motion. This is the main source of residual vibration observed in this robot.

The robot operates with two degrees of freedom: extension and rotation. Extension is achieved by directing the two stepper motors to rotate in different directions at the same speed, causing the wafer to move either away from or toward the center of the magnet retainers. Rotation is achieved by commanding the two stepper motors to rotate in the same directions at the same speed, thereby rotating the wafer about the center of the magnet retainers.

To streamline the kinematic analysis, polar coordinates is employed as depicted in Fig. 3, with the central point anchored at the center of the magnetic retainers. The radial direction, denoted as r, is the direction of the extension motion and the tangential direction, denoted as θ, is the direction perpendicular to the radial direction. This notation will also be utilized in subsequent sections.

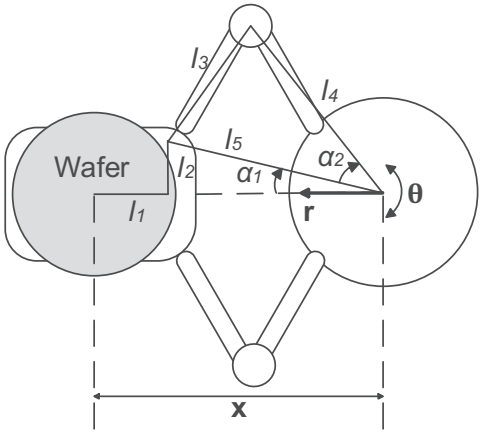

FIGURE 3: Robot kinematics

The sum of α_1 and α_2 is the angle commanded to the motors. The angle α_1 and α_2 can be expressed as functions of the distance between the center of the magnetic retainer and the center of the wafer, denoted as x, as shown in Eq. (1) to Eq. (3).

$$\alpha_1 = atan\left(\frac{l_2}{x - l_1}\right) \tag{1}$$

$$\alpha_2 = acos\left(\frac{l_5^2 + l_4^2 - l_3^2}{2 l_4 l_5}\right) \tag{2}$$

$$l_5 = \sqrt{(x - l_1)^2 + l_2^2} \tag{3}$$

Equations (1) to (3) enable us to determine the angle to command to the motors, given the commanded distance x.

2.2 Laser Sensor and Data Logger

A laser sensor, Keyence LK-G5000, was used to quantify the vibrational characteristic of the robot. The sensor offers a measuring range of 20mm when it is positioned 50mm away from the measuring surface, with a measuring resolution of 0.025 μm, sampled every 1 ms.

A data logger was utilized for the automatic acquisition of measurement data. The data logger receives a trigger signal from the motor driver and begins data logging when the robot is commanded to move. The acquired data are stored in the host PC for future analysis.

2.3 Target Controller and Motor Driver

The target controller and motor driver for the robot (Fig. 1) are integrated. The target controller communicates with the host PC/Matlab via EtherCAT, enabling high-speed communication for real-time control. It allows synchronized and precise control of the wafer-handling robot with existing ethernet infrastructure, simplifying the integration between the target controller and the host PC.

The target controller receives discrete commands in polar coordinate (e.g. r and θ) and convert them into motor angle commands (e.g. $\alpha_1 + \alpha_2$) for the stepper motors using Eq. 1-3.

2.4 Accelerometer

An ADXL345 accelerometer was installed on the end effector to measure the frequency responses of the robot in the r direction and the θ direction. The measured data served as a basis to determine the resonance frequency for input shaping control. Fig. 4 illustrates the configuration of the accelerometer. The robot is commanded to vibrate in either the r or the θ direction, allowing for the systematic collection of acceleration data in these directions.

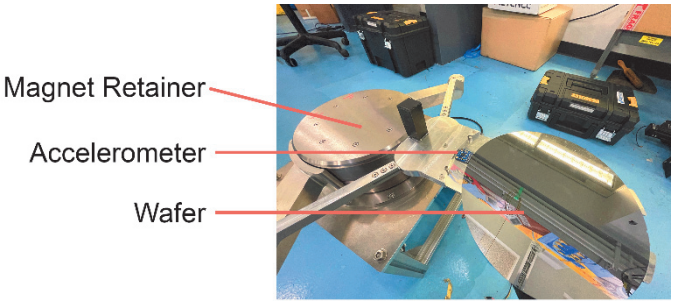

FIGURE 4: Accelerometer Setup

3. INPUT SHAPING CONTROL

In this research, zero vibration derivative (ZVD) input shapers are selected because they provide vibration suppression with high robustness [9]. The implementation of a ZVD shaper is composed of three impulses with magnitude A_i at time t_i for i =1,2,3 [10]:

$$A_1 = \frac{1}{K^2+2K+1}, t_1 = 0 \quad (5)$$

$$A_2 = \frac{2K}{K^2+2K+1}, t_2 = \frac{\pi}{\omega_n\sqrt{1-\zeta^2}} \quad (6)$$

$$A_3 = \frac{K^2}{K^2+2K+1}, t_3 = \frac{2\pi}{\omega_n\sqrt{1-\zeta^2}} \quad (7)$$

$$K = e^{-\frac{\zeta\omega_n}{\sqrt{1-\zeta^2}}} \quad (8)$$

where ω_n is the natural frequency and ζ is the damping ratio. The system parameters of the wafer-handling robot depend on the position of the blade. The resonance frequency ω_r was obtained by commanding sine sweeps to the robot where the frequency response was captured by the accelerometer. These obtained system parameters were then used to shape the input command for the robot to reduce tracking errors. Fig. 5 shows the resonance frequencies in the r and θ directions with respect to different positions (x) collected by the accelerometer. The data was used to design the ZVD shaper.

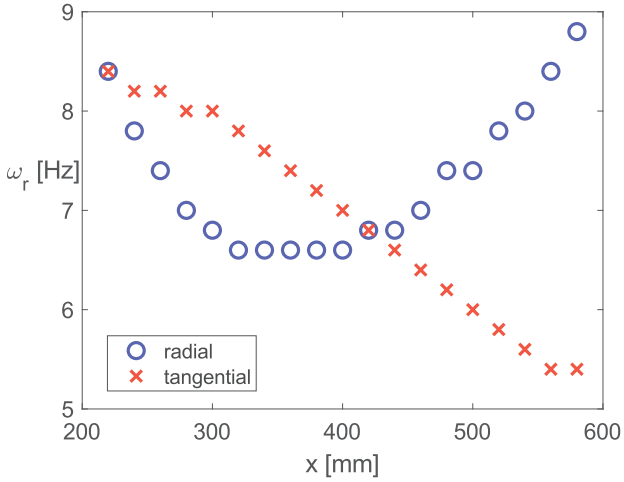

FIGURE 5: Resonance frequency in radial and tangential directions as functions of distance x (see Fig. 3)

4. EXPERIMENTAL RESULTS

The experimental findings in this section are segmented into two categories: rotation and extension. To ensure consistency, the robot was commanded to execute identical movements at least ten times. Motions with and without input shaping are displayed together in a single figure. To account for the sensor's restricted measurement range, the horizontal axis for each figure initiates from the point when the measuring surface (see Fig. 1) first enters the sensor's range.

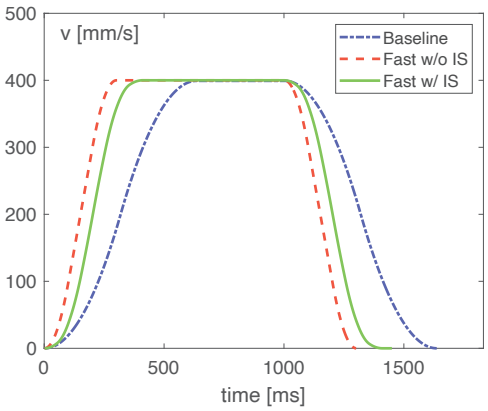

FIGURE 6: Speed profiles for commanding the robot to fully extend from fully retracted position in this study

TABLE 1: Parameters for the speed profiles in Figure 6

Profile	Max Speed (mm/s)	Max Accel (mm/s^2)	Max Jerk (mm/s^3)	Travel Time (ms)
Baseline	400	1500	4000	1687
Fast w/o IS	400	2000	20000	1351
Fast w/ IS	400	1958	15541	1411

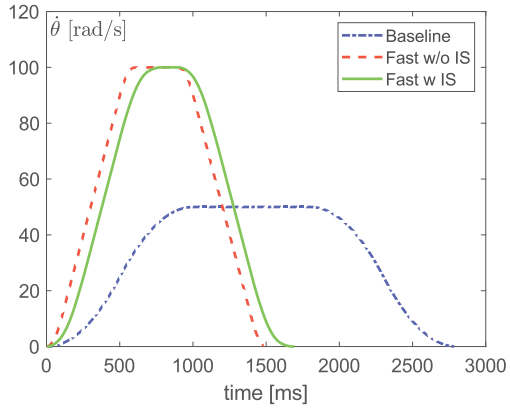

FIGURE 7: Speed profiles for commanding the robot to rotate in this study

TABLE 2: Parameters for the speed profiles in Figure 7

Profile	Max Speed (deg/s)	Max Accel (deg/s^2)	Max Jerk (deg/s^3)	Travel Time (ms)
Baseline	50	200	200	2800
Fast w/o IS	100	200	2000	1500
Fast w/ IS	100	200	1674	1635

Two distinct speed profiles are applied to the robot in this study: baseline and fast. The baseline and fast speed profiles involve commanding the stepper motors in such a way that the blade carrying the wafer accelerates uniformly, reaches and stays at a maximum speed, and then uniformly decelerates, as illustrated in Fig. 6 and 7 above. Baseline speed is chosen slow enough that no significant vibration is measured at the end of each motion. On the other hand, when the robot is commanded to travel at a faster speed, notable vibration is observed, as shown in subsequent sections. Table 1 and 2 provide details on the maximum speed, acceleration, jerk, and total traveling time of the baseline and fast motions.

4.1 Rotation

The robot barely vibrates when it is fully retracted during rotation. The amount of vibration observed increases as the distance of the end effector and the origin increases. Therefore,

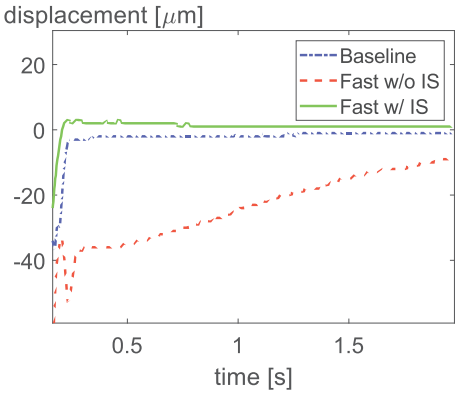

FIGURE 8: Displacement in r direction during rotation

with the center of the wafer 580 mm away from the origin when it is fully extended, the robot was commanded to rotate 90 degrees counter-clockwise to demonstrate the effect of IS. The displacements of the blade were measured in the r and θ directions, as shown in Fig. 8 and 9.

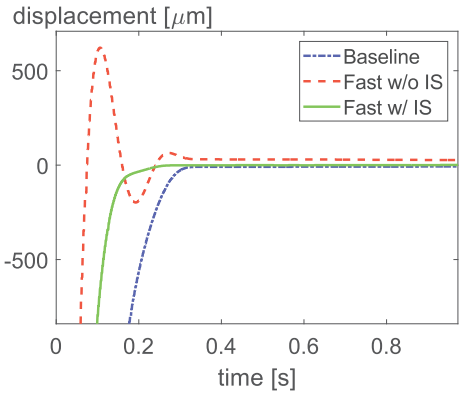

FIGURE 9: Displacement in θ direction during rotation

4.2 Extension

The robot was commanded to fully extend (x=600mm) from its fully retracted position (x=180mm). The reason for this selection is in practice, a cassette located at the robot's full reach is at risk of collision if vibration exists. The displacements of the blade were measured in the r and θ directions.

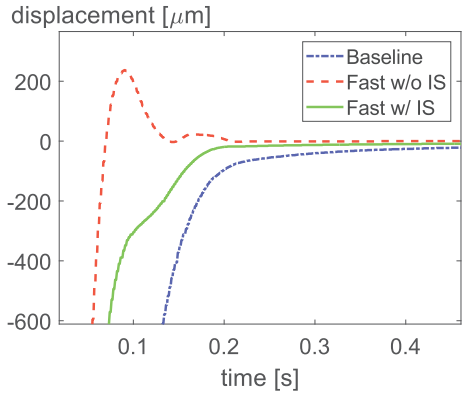

FIGURE 10: Displacement in r direction during extension

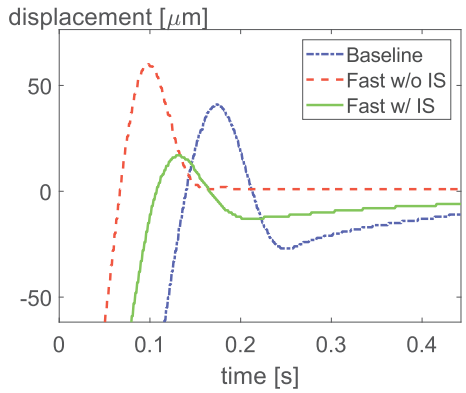

FIGURE 11: Displacement in θ direction during extension

In Figures 8 to 11, the laser sensor was fixed at a distance of 50 mm away from the final position of the blade. As the sensor has a measuring range of only 40 mm to 60 mm away from the sensor, it is not capable of measuring the distance between the blade from the origin of the robot (x in Fig. 3). The displacement along the vertical axis represents the blade's proximity to the sensor with an offset of 50 mm. When the blade moves closer to the sensor, the sensor outputs a positive value; when the blade moves farther away from the sensor, the sensor outputs a negative value.

5. DISCUSSION

Figure 9 depicts a substantial reduction in vibration observed during the rotation of the wafer-handling robot. When the robot is rotating at high speed, a rotational mode revolving about the center of the robot was excited, resulting in an overshoot up to 600μm. The ZVD shaper effectively eliminates the vibration. The frequency of the overshoot in Fig. 9 corresponds to the frequency of the vibration in Fig. 8 when the robot is rotating fast. This implies that the vibration mode excited during rotation induces displacements in both the r and θ directions. In Fig. 8, even after both actuators stopped moving, the blade kept drifting slowly towards zero when the robot was operating under fast speed. The reasons for this phenomenon remain unclear, yet the motion is undesirable. Interestingly, it is eliminated by the ZVD input shaper.

In the case of extension in Figures 10 and 11, the standard ZVD shaper has limited impact on the robot's motion. The shaper was able to eliminate the overshoot in the r direction, as shown in Fig 10. However, in Fig. 11, the ZVD shaper was shown to be not as effective as compared to Fig. 9 when the robot was rotating. The overshoot persists even when the speed, acceleration and jerk of the motion are decreased. As shown in Fig. 7, the natural frequency of the vibration during extension varies with position, and hence time. The ZVD shaper used for the extension motion was designed with the natural frequency corresponding to fully extended position. The relatively poor effectiveness of the ZVD input shaper during extension is likely due to its inability to handle varying natural frequencies.

6. CONCLUSION

This paper has carried out a preliminary investigation into input shaping as a tool to mitigate residual vibration in frog-leg robots used for silicon wafer-handling. Two motions of the frog-leg robot were investigated: rotational and extensional motions. A ZVD input shaper was shown to effectively suppress residual vibration during the rotational motion, allowing vibration-free motions at high speed. However, the ZVD input shaper was not as effective in mitigating residual vibration during the extensional motion. A likely reason for the ineffectiveness of the ZVD input shaper is its inability to handle the significant changes in vibration frequency that occur during extension. To address this weakness, future work will explore two variations of input shaping: an extra insensitive (EI) shaper [12] and a time-varying shaper [8]. EI shapers provide vibration suppression over a large frequency range, while time-varying input shapers provide vibration suppression for changing vibration frequencies.

ACKNOWLEDGEMENTS

The authors would like to thank Dr. Md Moktadir Alam for his help with editing the manuscript and for his useful feedback on the writing of the paper. They would also like to thank Epicrew Corporation for sponsoring this research project.

REFERENCES

[1] Chen, D., Tang, L., Cong, D., and Qiao, J. (2023) AcArm: A Novel Semiconductor Wafer Handling Robot. *China Semiconductor Technology International Conference (CSTIC)*, IEEE, Shanghai, China, 1–3.

[2] Yu, X., Wang, C., Zhao, Y., and Tomizuka, M. (2015) Controller Design and Optimal Tuning of a Wafer Handling Robot. *IEEE International Conference on Automation Science and Engineering (CASE)*, IEEE, Gothenburg, Sweden, 640–646.

[3] Li, H., Le, M. D., Gong Z. M., and Lin, W. (2009) Motion Profile Design to Reduce Residual Vibration of High-Speed Positioning Stages. *IEEE/ASME Transactions on Mechatronics*, April, 14(2), 264-269.

[4] Liu, Y., Cao, Y., Sun, L., and Zheng, X. (2010) Accurate and Steady Control on Trajectory Tracking for the Wafer Transfer Robot. *Industrial Robot: An International Journal*, 37(6), 552–561.

[5] Liu, Y., Cao, Y., Sun, L., and Zheng, X. (2010) Vibration suppression for wafer transfer robot during trajectory tracking. *2010 IEEE International Conference on Mechatronics and Automation*, Xi'an, China, 741-746.

[6] Aribowo, W., Yamashita, T., Terashima, K., Masui, Y., Saeki, T., Kamigaki, T., Kawamura H. (2011) Vibration Control of Semiconductor Wafer Transfer Robot by Building an Integrated Tool of Parameter Identification and Input Shaping. *IFAC Proceedings Volumes*, 44(1), 2011, 14367-14373.

[7] Wang, Z, Wang, C, and Tomizuka, M. (2015) Active Wide-Band Vibration Rejection for Semiconductor Manufacturing Robots. *Dynamic Systems and Control Conference*, Columbus, Ohio, USA.

[8] Wang, Z, Wang, C, and Tomizuka, M. (2015) Vibration cancellation of semiconductor manufacturing robots. *Manufacturing Letters*, vol. 4, 6-9.

[9] Singh, T., and Singhose, W. (2002) Input shaping/time delay control of maneuvering flexible structures. *Proceedings of the 2002 American Control Conference,* IEEE, Anchorage, AK, USA, 1717-1731.

[10] Singer, N., and Seering, W.P. (1990) Preshaping command inputs to reduce system vibration. *ASME Journal of Dynamic Systems, Measurement, and Control*, March, 112(1), 76-82.

[11] Thomsen, D.K., Søe-Knudsen, R., Brandt, D., Balling O., and Zhang, X. (2019) Smooth online time-varying input shaping with fractional delay FIR filtering. *Control Engineering Practice*, vol. 88, 21-37.

[12] Vaughan, J., Yano, A., and Singhose, W. (2008) Comparison of Robust Input Shapers. *Journal of Sound and Vibration*, September, 315(4-5), 797-815.